J. Phys. D: Appl. Phys. **32** (1999) 219–226. Printed in the UK PII: S0022-3727(99)96851-1

Electrostatic discharges and multifractal analysis of their Lichtenberg figures

T Ficker

Department of Physics, Technical University, Žižkova 17, CZ-602 00 Brno, Czech Republic

Received 17 August 1998, in final form 30 September 1998

Abstract. Morphological features of Lichtenberg figures created by electrostatic separation discharges on the surfaces of electret samples have been studied by means of multifractal analysis. The monofractal ramification of surface positive-channel streamers has been confirmed and found to be dependent on actual experimental conditions. For the lower level of electret saturation used, the fractal dimension $D \approx 1.4$ of the surface Lichtenberg channels has been obtained. Various registration features of electret and non-electret samples have been discussed and illustrated.

1. Introduction

Typical electrostatic discharges arise during separation of a charged sheet of a highly resistive material from a grounded object. Such electrostatic discharges are sometimes called 'separation discharges'. Their damaging effects on some industrial products are well known: they degrade tracks on paper and photographic materials, induce noise in electronic components or cause inconvenience for the human body, to mention some of them. Electrostatic discharges can sometimes cause hazards in spaces where explosive vapours are present. The study of these discharges is therefore useful from the technological point of view. In addition, their discharge mechanism comprises many interesting features not only from plasma physics but also from solid state and surface physics.

Electrostatic discharges often assume the form of surface discharges when charge carriers are forced to propagate along a dielectric surface. In such cases many carriers are trapped on the highly resistive surface and create latent invisible tracks, which can be visualized by powdering the surface. The microscopic powder particles are immobilized on the surface by strong electrostatic bonds caused by the trapped carriers. When the surplus powder is gently blown away, the powder that remains adhering to the surface forms characteristic patterns. These characteristic visible powder tracks are called 'Lichtenberg figures' after their discoverer [1]. The Lichtenberg figures can be also created by means of photographic films. It is believed [2] that images in the film are identical in size and shape to the 'powder figures' on the dielectric surface if both the registration materials have experienced the same exposure to the electrical discharges. Since their finding the Lichtenberg figures have been used many times [2–11] to study gaseous discharges on the surface of dielectrics.

The majority of the studies dealing with Lichtenberg figures has used point-to-plane electrode systems and short voltage pulses in the microsecond and nanosecond regimes. The consequence of such special experimental arrangements is the characteristic form of the corresponding Lichtenberg figures: a single circular star-shaped channel structure for a positive pulse (positive streamers) and a single circular spot built up in a practically continuous manner for a negative pulse (negative streamers). Only a few studies avoid this traditional experimental arrangement: Bertein [3] has used a dc HV source and three different types of electrode systems: parallel, dihedron and plane-to-cone assemblies with larger discharge gaps (0.1–2 cm). Takahashi *et al* [8] have studied the Lichtenberg figures created by electrostatic separation discharges by means of a quite untraditional experimental arrangement. They have separated corona-charged sheets of polymethylacrylate from a rotating grounded metal cylinder. The Lichtenberg figures have been recorded by the powder technique as well as with a video camera. All these studies show that the positive streamers present a clearly distinguishable channel structure whereas negative streamers manifest a very fine and nearly continuous structure.

Our experimental arrangement consists of a tight plane-to-plane electrode system and a dc high voltage applied for various time periods ranging from several minutes to many hours. This arrangement resembles that used for forming electrets; moreover, the chosen highly resistive dielectric samples—sheets of polyethyleneterephthalate—are good electrets. However, charging of the samples is performed not at high temperatures as with the usual means of electret forming but rather at common room temperatures. When the sheet of polymer is separated from the grounded planar electrode, the electrostatic discharges 'draw' latent Lichtenberg figures on the surface of the polymer.

The morphology of Lichtenberg figures was a subject of interest many times in the past. With the appearance of fractal

0022-3727/99/030219+08$19.50

geometry morphological studies became more sophisticated and more exact. The pioneering work of Niemeyer *et al* [6] has shown that random structures of positive-corona streamers form fractal patterns on the dielectric surface and that these patterns can be modelled on a computer. These facts have been verified later many times by other authors [9–18]. Nevertheless, most authors of the work published on the morphology of electrical discharges prefer computer simulations over the direct fractal analysis of experimental data.

This contribution is aimed at the direct analysis of the Lichtenberg figures created by electrostatic separation discharges. The general multifractal formalism [19–41] in the modification of Voss [36] is used to perform the multifractal image analysis of surface discharge patterns.

2. The experimental arrangement

Highly resistive polymeric sheets of amorphous polyethyleneterephthalate (PET-a) have been cleaned carefully with ethanol and then inserted between two short-circuited copper plates for 24 h to eliminate surface charges. PET-a sheets 0.180 mm thick have been pressed between flat bronze electrodes of diameters $\Phi_1 = 20$ mm and $\Phi_2 = 40$ mm. The smaller electrode has been loaded with the negative electrical potential of -8.5 kV while the larger electrode has been grounded. The duration of application of HV has been chosen in the intervals of several minutes to hundreds of hours.

The field strength in the samples has not been tested separately but estimated only by means of elementary phenomenological considerations. The plane-parallel electrode system allows us to assume that there is a uniform field in the central region of electrodes while at their periphery a highly divergent field is expected. Supposing that polarization is the main mechanism for charging of samples, the external HV of 8.5 kV will cause a field strength of 14.31 kV mm^{-1} in a polyethyleneterephthalate sheet 0.18 mm thick with the relative permittivity $\varepsilon_r = 3.3$. Under identical suppositions the density of surface charges can be also estimated to be

$$\sigma_d = (\varepsilon_r - 1)\frac{\varepsilon_0}{t}U$$

$$\varepsilon_0 = 8.854 \times 10^{-12}\ \mathrm{F\ m^{-1}}$$

$$\varepsilon_r = 3.3$$

$$t = 0.18 \times 10^{-3}\ \mathrm{m}$$

$$U = 8.5 \times 10^{3}\ \mathrm{V}$$

$$\sigma \approx 961\ \mu\mathrm{C\ m^{-2}}. \qquad (1)$$

The polyethyleneterephthalate material is a well-known electret [42, 43] with aromatic and polar groups. The loading with HV causes its quasi-permanent charging, namely the active electret state. Two mechanisms leading to the electret state with PET-a have been reported [42, 43]: polarization of dipoles and redistribution of volume 'free' charges; each of them dominates at different temperatures of poling. Although our poling of PET-a takes place at room temperature ($\simeq 20\,^{\circ}$C), it can be anticipated that both mechanisms participate more or less in this charging process. However, the density of remanent surface charges on the sample after switching off the external electrical field hardly reaches the estimated value (1), $\sigma_d \approx 961\ \mu$C m^{-2}, holding for an ideal dielectric under HV stress. The remanent charge density is supposed smaller but is still larger than 100 μC m^{-2}, which is the approximate limiting value necessary for the appearance of surface positive streamers of separation discharges reported by Takahashi *et al* [8]. In addition, the actual value of the remanent surface charge density will be dependent on the duration of poling of the sample. There will be a critical time interval ensuring charge saturation σ_s at constant HV; that is, for all poling intervals larger than that which is critical the remanent charge densities σ_s will be identical. Such a behaviour of surface charges is observed with standard electrets. The resulting electret state after removal of the HV electrode is such that the PET-a sheet is attached to the grounded electrode owing to electrostatic forces, which can be easily tested when separating the sheet from the earthed electrode.

During separation of two inversely charged surfaces the wedge-shaped air discharge gap successively increases and, when it attains an optimal Paschen value, an electrostatic discharge occurs. Since the grounded electrode bears positive charges and the attached surface of the polymeric sheet negative ones, the positive streamers will be directed towards the polymeric surface while negative streamers are directed towards the surface of the metallic electrode. Hence the powder technique will reveal Lichtenberg figures of positive channel streamers embedded within the background of the negative remanent electret charge on the polymeric surface. The commercial black powder 'Minolta toner IV' made from styrene acrylate copolymer filled with carbon black, pigment, iron oxide and silica has been used to develop the figures. The discharge figures have been scanned with the resolution of 1200 dpi and their digital images processed; the channel structure has been extracted from the background and then subjected to the multifractal analysis software.

3. Multifractal analysis

From the very beginning of the 1980s multifractal computations [19–41] have been used as the basic tool for the morphological analysis of complex objects embedded in Euclidean space. For multifractal analysis the Euclidean space of the topological dimension E is partitioned into an E-dimensional grid whose basic cell is of a linear size ε. One of the topological measures used in this field is the measure [36] $\mu_m(\varepsilon, q)$ defined by means of probability moments:

$$\mu_m(\varepsilon, q) \approx m^q P_m(\varepsilon) \qquad (2)$$

where $P_m(\varepsilon)$ can be regarded as an 'occupation' probability and m an 'occupation' number:

$$P_m(\varepsilon) = \frac{N_m(\varepsilon)}{N_o(\varepsilon)} \qquad \sum_m P_m(\varepsilon) = 1. \qquad (3)$$

The 'occupation' integer m represents the number of points within one cell. The symbol $N_m(\varepsilon)$ expresses the number of cells containing m points and $N_o(\varepsilon)$ is the number of cells

containing at least one point; that is, it represents the total number of occupied cells.

The goal of the multifractal analysis is to determine one of the three existing multifractal spectra. The most frequently used spectrum is that of generalized dimension D_q:

$$D_q = \lim_{q^* \to q} \frac{\partial \ln[\sum_m \mu(\varepsilon, q^*)]}{q^* \partial \ln \varepsilon} = \lim_{q^* \to q} \frac{\partial \ln M(\varepsilon, q^*)}{q^* \partial \ln \varepsilon}. \quad (4)$$

The fractal objects are assumed in the form of graphical bitmap files that have been created by digitizing pictures (in our case Lichtenberg figures). The plane of graphical pixels (points) representing the fractal set is covered with an ε grid whose basic cell is of the linear size ε pixels. On this grid the measure (2) is computed. Since the covering of the plane with a grid is arbitrary and the way of covering the plane should not influence the results, we realize several coverings in order to find the average value of the partition sum $M_q(\varepsilon)$. For each ε grid there are ε^2 independent coverings generated by shifting the grid origin within the first ε cell

$$M_q(\varepsilon) = \frac{1}{\varepsilon^2} \sum_{j=1}^{\varepsilon^2} M_j(\varepsilon, q). \quad (5)$$

Such a procedure requires the fractal set to be embedded in a larger grid that allows one to move the origin without the loss of any part of the fractal object. The averages $M_q(\varepsilon)$ are estimated for a series of ε grids and the slopes in the bilogarithmic plot $\ln M_q(\varepsilon) \simeq \ln \varepsilon$ are calculated using the linear regression method. These slopes divided by the corresponding q values represent the dimensions D_q (4). Different D_q values for an analysed object indicate multifractal behaviour whereas identical values signify simple fractal features.

The algorithm described above has been implemented by means of the software tool Delphi 3. The created computer program is able to run on the NT system or on Windows 95/98.

4. Results and discussion

The necessary prerequisite for revealing Lichtenberg figures in our experimental arrangement is the separation of the charged PET-a sheet from the grounded electrode. If the separation were not performed and the sheet remained attached to the metallic electrode, the corresponding powder figure (powdering on the top surface of the sheet) would be a nearly homogeneous black background of the electret remanent charge without any tracks of positive streamer channels. As soon as the separation starts and 'invisible' discharges take place, miniature geysers of expelled powder particles signifying the formation of channels can be seen. Nevertheless, in our experimental work the powdering was applied to the polymeric surface attached to the grounded electrode after the separation had been performed.

Figures 1–6 show surface structures created by separation electrostatic discharges in order of increasing time of electret poling. For longer times of poling (longer that 2 h) clear positive streamer channels appear (figure 3–6) whereas shorter times of poling (shorter than 30 min) yield only an indistinct channel structure (figure 1). Extremely great intervals of poling (74.5 and 295.25 h—figures 5 and 6) do not give sharper or more ramified channel structure than those obtained with 2 and 3 h intervals of poling (figures 3 and 4). From these facts it follows that, in our case, the critical time necessary for attaining saturation of the electret surface charge approaches 2 h.

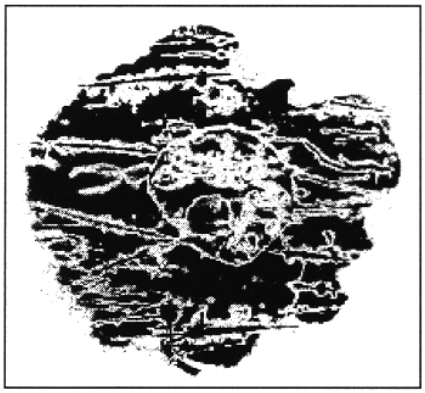

Figure 1. The electrostatic discharge structure for a poling time of 1 min.

Figure 2. The electrostatic discharge structure for a poling time of 30 min.

In figures 3–6 it is interesting to note the characteristic features of the channel structure and the black background. Although both regions are black, they bear opposite charges: the channel objects are positively charged while the background is negatively charged. The reason for that lies in the dielectric nature of the powder particles used that are attracted equivalently by both types of charges regardless of their signs, as we have verified by separate experiments. In addition, the separate experiments with the mixture of red-coloured lead oxide (bearing a positive charge) and yellow–white sulphur (bearing a negative charge) confirm that the polarities of the two regions are different. Nevertheless, interfaces between positive channels and negative background, which are manifested in the form of narrow white strips following the channels, represent neutral zones between the two charged regions.

To the best of our knowledge, the first author who reported the channel structure of electrostatic separation discharges on the surface of polyethyleneterephthalate was

Figure 3. The electrostatic discharge structure for a poling time of 2.2 h. (a) the original structure and (b) the extracted channel structure ($D = 1.36 \pm 0.02$).

Figure 4. The electrostatic discharge structure for a poling time of 3.2 h. (a) the original structure and (b) the extracted channel structure ($D = 1.45 \pm 0.03$).

Bertein [3]. She presented a picture (figure 7 in [3]) showing a 'charge distribution obtained when a negatively charged foil of Mylar is removed far from an earthed plate'. The clearly depicted and ramified channel structure is very similar to that in our figures 3–6. Similar pictures are available also in the detailed study of these discharges published by Takahashi *et al* [8]. They classified the separation discharges into two groups: (i) 'micro-discharges' which form some diffuse spots instead of a channel structure and (ii) 'major discharges' with a pronounced channel structure. According to these authors it is the initial surface charge density σ that discriminates the two discharge modes. For smaller surface densities $\sigma < 100\ \mu\text{C m}^{-2}$ there appears an indistinct channel structure of micro-discharges (figures 3(e) and (f) in [8]) which might correspond to our figure 1. For very small densities $\sigma < 12\ \mu\text{C m}^{-2}$ they encountered no separation discharges. For the limiting value $\sigma \approx 100\ \mu\text{C m}^{-2}$ these authors reported a channel structure with a characteristic length of several millimetres, which might be the case of our figure 2. For larger densities $\sigma > 100\ \mu\text{C m}^{-2}$ they supposed that there would be clearly resolved channel structures; for example, at $\sigma \approx 150\ \mu\text{C m}^{-2}$ the characteristic length of their streamers was about 90 mm. The length of our surface streamers is limited by the diameter of the earthed electrode (40 mm) but in all saturated cases (figures 3–6) the length of 40 mm has been observed, at least with some of the manifested channels, especially in figures 5 and 6.

A further characteristic feature in the morphology of positive streamer channels is their ramification. The branching of the surface channels determines the geometry of the structure. An abundant ramification, when branches thoroughly fill the surface, leads to the geometrical structure whose dimension D will approach that of a plane $D = 2$. On the other hand, with poor ramification, when branches arise scarcely and the structure reminds one of a group of simple linear channels, the corresponding dimension can be expected to be close to that of a line $D_{lin} = 1$. Therefore, the interval $\langle 1, 2\rangle$ represents all possible values of dimensions D of the surface positive streamers. The actual geometrical dimension D for a given structure can be obtained from the multifractal analysis in the form of the Hausdorff–Besicovitch dimension D_{-1} [45]. To analyse our

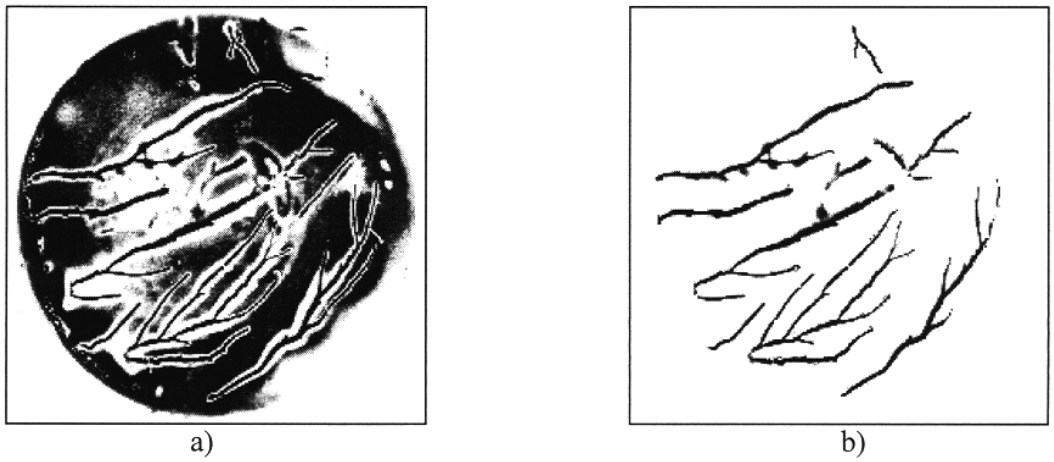

Figure 5. The electrostatic discharge structure for a poling time of 74.5 h. (a) the original structure and (b) the extracted channel structure ($D = 1.45 \pm 0.02$).

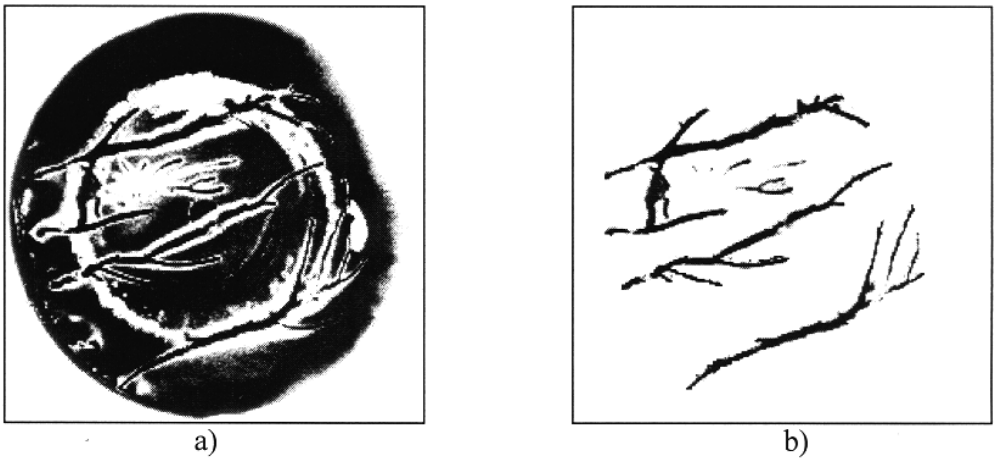

Figure 6. The electrostatic discharge structure for a poling time of 295.25 h. (a) the original structure and (b) the extracted channel structure ($D = 1.32 \pm 0.03$).

surface streamers, it was necessary to extract the channel structure from the background of the remanent electret surface charge. This extraction has been performed within digital processing of the scanned images and the extracted structures are depicted in figures 3(b)–6(b). The results of the corresponding multifractal analysis have shown that the studied structures manifest fractal rather than multifractal features so that the spectrum of the generalized dimensions D_q reduces to a single representative value D for all q. The actual values of the dimensions D for the structures from figures 3–6(b) are given in the last column of table 1 and are in the range 1.3–1.5 within the limiting statistical error of 2%. For the sake of comparison the last but one column of table 1 contains the fractal dimensions of the whole structure including the black background. These dimensions are higher (1.7–1.8), which could be expected since the whole structure fills the dielectric surface better than does that without the background.

The first authors who recognized possible fractal features of a surface discharge channel structure and tried to estimate its fractal dimension were Niemeyer *et al* [6]. Their radially shaped channel structure of the Lichtenberg figure was created on a 2 mm glass plate in 0.3 MPa SF_6 by an applied voltage pulse of 30 kV in 1 μs; a rod-to-plane electrode arrangement was used. These authors visually analysed the obtained radial structure and for the estimation of its dimension they counted the number of branches n at various radii r:

$$n(r) \simeq r^{D-1}. \tag{6}$$

A careful counting of the number $n(r)$ of branches for various radial distances r and a bilogarithmic plot of these data allowed them to determine the dimension $D \approx 1.7$. This higher value of the dimension corresponds to a more ramified channel structure, which can be easily checked by visual inspection of their structure (figure 1 in [6]) and those depicted in our figures 3–6. A similar manual monofractal analysis was repeated later [9] with practically identical results. The authors of [6] also started computer simulations of the surface channel structure. Many followers appeared in this field [12–18]. The dimensions from computer simulations exhibit a large variety of values according to the model parameters chosen. It is possible to find structures with restricted ramification [10], namely, with a lower dimension

Table 1. Results of multifractal analysis and physical conditions of the experiment.

	Experimental conditions		Dimension of the total structure	Dimension of the channel structure
Figure 1	$\varphi = 39\%$ $p = 102.5$ kPa $T = 23\,^{\circ}$C	8.5 kV 1 min	1.829 ± 0.005	
Figure 2	$\varphi = 46\%$ $p = 102.4$ kPa $T = 21.4\,^{\circ}$C	8.5 kV 30 min	1.70 ± 0.02	
Figure 3	$\varphi = 56\%$ $p = 102.3$ kPa $T = 20.6\,^{\circ}$C	8.5 kPa 2.2 h	1.73 ± 0.02	1.36 ± 0.02
Figure 4	$\varphi = 50\,^{\circ}$C $p = 102.5$ kPa $T = 21\,^{\circ}$C	8.5 kV 3.2 h	1.794 ± 0.005	1.45 ± 0.03
Figure 5	$\varphi = 38\%$ $p = 102.2$ kPa $T = 19.5\,^{\circ}$C	8.5 kV 74.5 h	1.825 ± 0.009	1.45 ± 0.02
Figure 6	$\varphi = 27\%$ $p = 102.0$ kPa $T = 21\,^{\circ}$C	8.5 kV 295.25 h	1.814 ± 0.006	1.32 ± 0.03

$D \approx 1.46$ [10], which is close to our values (the last column of table 1), or more ramified structures $D \approx 1.75$ [6, 10] or even very branched structures with $D \approx 1.8$–1.96 [6, 14]. Although a recent view [44] of the previous computer models [6] was slightly critical, it should be remembered that, in the field of stochastic processes, these models efficiently assisted one in establishing the new concept of fractal geometry that later proved to be very fruitful and useful in spite of various obstacles appearing during its introduction. In addition, computer models verified that ramification and, therefore, also fractal dimensions are strongly dependent on the model parameters that approximate the physical conditions under which a discharge experiment has been realized. Although much work in this field has been done, one important question still remains: what physical parameters influence the ramification of the channel structure and what mechanisms participate?

The original computer model of Niemeyer *et al* [6] solved the problem of ramification by introducing the 'growth' probability p dependent on a local electrical field E:

$$p \propto E^{\eta} \tag{7}$$

where η is a model parameter. In consequence of the simplifying simulation steps the dimension D of the resulted structure is dependent solely on the model parameter η, namely, $D(\eta)$, although there is experimental evidence [3, 8] that the branching depends on more than one parameter. Let us mention some of them: the thickness ratio of the discharge gap and the dielectric layer, the electronegativity of the gas used and the external voltage chosen. The dependence on the external voltage for the case of our surface electrostatic separation discharges actually means the dependence on the electret charge density σ. This fact can be illustrated by reference to figures 2 and 3. In figure 2 the practically unramified and weakly resolved channel structure embedded in an unsaturated electret charge can be seen whereas in figures 3–6 clearly branched sharp channel structures accompanied by saturated electret surface charges are manifested. The saturation states of the structures in figures 3–6 imply that they have mutually similar degrees of ramification, which is reflected in the similar values (≈1.4) of their fractal dimensions (the last column of table 1).

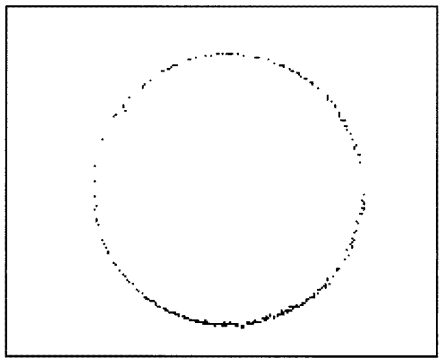

Figure 7. Direct micro-discharges at the grounded electrode.

Finally, it might be of interest to mention another feature of discharge figures that is at first sight surprising: the channel structure does not appear when one is using a photographic film instead of the dielectric sample. The reason is natural. The photographic emulsion is not an electret that can be charged so that no surface charge density remains after removal of the HV electrode. Thus, no electrostatic discharges occur on separating the photographic film from the grounded electrode. Nevertheless, the developed film reveals numerous small discharge spots (figure 7) at the periphery of the electrode to which the photosensitive emulsion has been attached. The 'slight' micro-discharges at the edges of electrodes are initiated when a HV electrical field acts on a sample. The micro-discharges are of the same nature as the so-called 'partial' discharges that can cause successive degradation of metal insulator interfaces. We have studied the fractal features of amplitude and time statistics of partial

micro-discharges previously [46] but without morphological connections. The partial micro-discharges 'follow' the shape of metallic edges so that the discharge spots 'draw' the circular outlines of the parent electrode. Using lower values of HV and a shorter exposure time (several minutes) the discharge spots are scarcely scattered along the circle like single points. Topologically this situation represents a fractal dimension of zero. With increasing HV and exposure time the points will tend to draw the circle more continuously and the fractal dimension will approach the dimension of a linear object, $D = 1$. This is the case of our structure in figure 7 (4 kV and 90 min exposure) whose dimension $D = 0.987 \pm 0.009$ is very close to unity. At still higher fields and exposure times it can be anticipated that 'widening' of the discharge circle into a circular strip or band will occur, with the dimension approaching that of a two-dimensional object, $D = 2$. Nevertheless, such intensively loaded films suffer overexposure, which makes them hard to process. For completeness a remaining question should be answered; namely that of why the dielectric polyethyleneterephthalate samples are not affected by these fine micro-discharges. Undoubtedly, they experience impacts of the micro-discharges during HV loading but the corresponding charge transferred to the surface of a dielectric is not able to compete with the high density of dielectric surface charge (see equation (1)). For an extraordinarily long HV loading (hundreds of hours) the influence of micro-discharges is not negligible and can be observed also in powder figures; see figure 5(a) that contains the white neutral strip around the smaller HV electrode drown inside the black background representing the image of the larger grounded electrode.

5. Conclusion

This contribution has discussed morphological features of Lichtenberg figures created by electrostatic separation discharges on the surface of electret samples. Under the given experimental conditions, restricted ramifications of the channel structure of positive streamers have been observed and the corresponding fractal dimensions estimated. A saturated electret state ensures that the formation of channels with 'self-similar' ramification of a characteristic fractal dimension occurs. In our case, with PET-a samples the saturation has been reached at room temperatures, with the field strength about 14 kV mm^{-1} and within a poling time of about 2 h. The attained density of remanent electret surface charge is supposed to be higher than 100 μC m^{-2} and has caused electrostatic separation discharges that have formed Lichtenberg positive channels with the average fractal dimension $D \approx 1.4$. It is expected that the electret states of higher saturation ($\sigma \gg 100$ μC m^{-2}) will provide Lichtenberg figures with more abundant and structured ramification possessing higher fractal dimensions. However, generally the fractal dimension of the surface Lichtenberg channels must lie in the interval $\langle 1, 2 \rangle$.

The samples with photographic emulsion do not exhibit any Lichtenberg channel that would be caused by electrostatic separation discharges since they are not electrets that are able to conserve a remanent electret charge and, thus, they cannot experience electrostatic separation discharges. However, they are able to register 'fine' partial micro-discharges running under the action of a HV field at the edges of electrodes. The micro-discharges 'dot' in a stochastic manner the outlines of metallic edges in the photographic emulsion and the developed small discharge spots more or less fill the surface of the film. The filling of the surface by discharge spots is governed by the actual experimental conditions and can vary from discontinuous fractal scattering of separate points through almost continuously filled linear outlines of electrodes up to densely filled area strips (bands). Such a variety of ways of filling the surface corresponds to the wider interval $\langle 0, 2 \rangle$ of fractal dimensions.

The fractal dimension seems to be a characteristic parameter classifying not only the amplitude distributions of partial discharges [46] but also the topology of surface streamers of separation discharges. This topology seems to be closely connected with the level of electret surface charge that is the main driving factor in the mechanism of electrostatic separation discharges.

Acknowledgments

This work was supported by the grant agency of the Czech Republic under grant 202/97/1407. Thanks are also due to Dr D Martišek for software work and Associate Professor M Druckmüller for digitizing pictures.

References

[1] Lichtenberg G C 1777 *Novi Comm. Soc. Reg. Sci. Gott.* **8** 168
[2] Morris A T 1951 *Br. J. Appl. Phys.* **2** 98
[3] Bertein H 1973 *J. Phys. D: Appl. Phys.* **6** 1910
[4] Murooka Y and Koyama S 1979 *J. Appl. Phys.* **50** 6200
[5] Nakanishi K, Yoshioka A, Shibuya Y and Nitta T 1982 Charge accumulation on spacer surface at dc stress in compressed SF_6 gas *Gaseous Dielectrics III* ed L G Christophorou (New York: Pergamon) p 365
[6] Niemeyer L, Pietronero L and Wiesmann H J 1984 *Phys. Rev. Lett.* **52** 1033
[7] Hidaka K and Murooka Y 1986 *J. Appl. Phys.* **59** 87
[8] Takahashi Y, Fujii H, Wakabayashi S, Hirano T and Kobayashi S 1989 *IEEE Trans. Electr. Insul.* **24** 573
[9] Niemeyer L 1991 *7th Int. Symp. on High Voltage Engineering, Dresden* p 937
[10] Femia N, Lupo G and Tucci V 1991 *7th Int. Symp. on High Voltage Engineering, Dresden* p 921
[11] Gallimberti I, Marchesi G and Niemeyer L 1991 *7th Int. Symp. on High Voltage Engineering, Dresden*
[12] Murat M 1985 *Phys. Rev.* B **32** 8420
[13] Fujimori S 1985 *Japan. J. Appl. Phys.* **24** 1198
[14] Satpathy S 1986 *Phys. Rev. Lett.* **57** 649
[15] Wiesmann H J and Zeller H R 1986 *J. Appl. Phys.* **60** 1770
[16] Evertsz C 1989 *J. Phys. A: Math. Gen.* **22** L1061
[17] Pietronero L and Wiesmann H J 1988 *Z. Phys.* B **70** 87
[18] Barclay A L, Sweeney P J, Dissado L A and Stevens G C 1990 *J. Phys. D: Appl. Phys.* **23** 1536
[19] Mandelbrot B B 1972 Possible refinement of the lognormal hypothesis concerning the distribution of energy dissipation in intermittent turbulence *Statistical Models and Turbulence* ed M Rosen and C Van Atta (New York: Springer) pp 333–51
[20] Mandelbrot B B 1974 *J. Fluid Mech.* **62** 331
[21] Mandelbrot B B 1983 *The Fractal Geometry of Nature* (New York: Freeman)

[22] Grassberger P 1983 *Phys. Lett.* A **97** 227
[23] Hentschel H G E and Procaccia I 1983 *Physica* **8** 435
[24] Grassberger P and Procaccia I 1983 *Physica* **9** 189
[25] Grassberger P and Procaccia I 1984 *Physica* D **13** 34
[26] Badii R and Politi A 1984 *Phys. Rev. Lett.* **52** 1661
[27] Badii R and Politi A 1985 *J. Stat. Phys.* **40** 725
[28] Frisch U and Parisi G 1985 On the singularity structure of fully developed turbulence *Turbulence and Predictability in Geophysical Fluid Dynamics and Climate Dynamics* ed M Ghil *et al* (New York: North-Holland) pp 84–8
[29] Jensen M H, Kadanoff L P, Libchaber A, Procaccia I and Stavans J 1985 *Phys. Rev. Lett.* **55** 2798
[30] Bensimon D, Jensen M H and Kadanoff L P 1986 *Phys. Rev.* A **33** 3622
[31] Halsey T C, Jensen M H, Kadanoff L P, Procaccia I and Shraiman B I 1986 *Phys. Rev.* A **33** 1141
[32] Glazier J A, Jensen M H, Libchaber A and Stavans J 1986 *Phys. Rev.* A **34** 1621
[33] Feigenbaum M J, Jensen M H and Procaccia I 1986 *Phys. Rev. Lett.* **57** 1503
[34] Chhabra A B and Jensen R V 1989 *Phys. Rev. Lett.* **62** 1327
[35] Chhabra A B, Menevean C, Jensen R V and Sreenivasan K R 1989 *Phys. Rev.* A **40** 5284
[36] Voss R F 1985 Random fractals: characterization and measurement *Scaling Phenomena in Disordered Systems* ed R Pynn and A Skjeltorp (New York: Plenum) pp 1–11
[37] Feder J 1988 *Fractals* (New York: Plenum) p 80
[38] Baumann G and Nonnenmacher T F 1989 Determination of fractal dimensions *Gli oggetti fractali in astrofisica, biologia, fisica e matematica* ed G A Losa *et al* (Locarno: Cerfim) pp 93–104
[39] Losa G A 1991 *Microsc. Elett.* **12** 118
[40] Bauman G, Barth A and Nonnenmacher T F 1993 Measuring fractal dimensions of cell contours: practical approaches and their limitations *Fractals in Biology and Medicine* ed G A Losa *et al* (Basel: Birkhäuser)
[41] Losa G A, Nonnenmacher T F and Weibel E R 1993 *Fractals in Biology and Medicine* (Basel: Birkhäuser)
[42] Belana J, Mudarra M, Calaf J, Cañadas J C and Menéndez E 1993 *IEEE Trans. Electr. Insul.* **28** 287
[43] Kressman R, Sessler G M and Günther P 1996 *IEEE Trans. Dielectr. Electr. Insul.* **3** 607
[44] Dodd S J, Dissado L A, Champion J V and Alison J M 1995 *Phys. Rev.* B **52** R16 985
[45] Ficker T 1989 *Phys. Rev.* A **40** 3444
[46] Ficker T 1995 *J. Appl. Phys.* **78** 5289